Astron. Astrophys. 312, 289–305 (1996)

ASTRONOMY AND ASTROPHYSICS

Ultraviolet processing of interstellar ice analogs

I. Pure ices

P.A. Gerakines[1,2], W.A. Schutte[1], and P. Ehrenfreund[1]

[1] Leiden Observatory, Postbus 9513, 2300 RA Leiden, The Netherlands
[2] Dept. of Physics, Applied Physics, & Astronomy, Rensselaer Polytechnic Institute, Troy, NY 12180, USA

Received 4 August 1995 / Accepted 4 January 1996

Abstract. Interstellar ices are chemically processed by ultraviolet (UV) radiation to form complex products, and models of UV photochemistry provide powerful tools for the interpretation of astronomical observations. We have performed UV photolysis experiments on pure 10 K samples of nine ices of molecules of astrophysical interest: H_2O, NH_3, CH_4, CO, CO_2, O_2, N_2, H_2CO, and CH_3OH. Destruction of these species by photochemical processes is discussed, and the cross-sections for destruction are estimated for use in chemical models. New molecules produced during photolysis are identified on the basis of their characteristic infrared features, and their chemical origins and astrophysical implications are discussed. Rates of formation are also estimated for first-order products. In experiments with CH_4 and with H_2CO, molecules with as many as 7 - 8 C atoms are produced. Such results may indicate how and why very complex organic molecules are formed in molecular mixtures characteristic of interstellar ice mantles.

Key words: ISM: molecules – dust, extinction – infrared: ISM: lines and bands – molecular data – molecular processes – methods: laboratory

1. Introduction

Molecules in the interstellar environment undergo chemical reactions driven by such forces as cosmic ray ionization, the interstellar radiation field, and shocks (due to supernovae and nearby star formation), and are constantly being destroyed and reformed by these processes. Observations of complex molecules in the interstellar medium (ISM) indicate a rich chemistry of diverse molecules. Such astronomical observations are complimented by chemical models which predict that a population of simple atomic species will eventually evolve into a complex chemistry (e.g. d'Hendecourt et al. 1986; Hasegawa et al. 1992; Shalabiea & Greenberg 1994). This often involves intricate chemical pathways whose endproducts bear little resemblance to the initial contents.

The solid phase of the dense ISM, in the form of dust grains and the ice mantles coating their surfaces, has long been observed through infrared (IR) absorption features towards lines of sight which intercept interstellar material. The fundamental vibrational modes of most molecules fall in the mid-infrared (2 - 25 μm), and the features of solid species may be discerned from corresponding gas-phase transitions since the rotational structure is suppressed and the peak wavelengths of the absorptions are shifted (sometimes by large amounts) from positions in the gas phase.

Some molecules which have been identified as important constituents of interstellar ice mantles by IR spectroscopy are H_2O (e.g., Willner et al. 1982; Smith et al. 1989), CO (e.g., Lacy et al. 1984; Whittet et al. 1989; Tielens et al. 1991), CH_3OH (Allamandola et al. 1992), H_2CO (Schutte et al. 1996), CH_4 (Boogert et al. 1996), and CO_2 (d'Hendecourt & Jourdain de Muizon 1989). Such ices, while present in dense clouds, would be subjected to ultraviolet (UV) radiation originating from internal sources (such as cosmic ray induced photons and embedded protostars) or from the penetration of the diffuse galactic radiation field (e.g., Greenberg 1973; Sternberg et al. 1987; Prasad & Tarafdar 1983; Schutte & Greenberg 1991 and references therein).

The cosmic ray induced UV flux internal to a dense cloud amounts to $\sim 10^3$ photons cm^{-2} s^{-1} ($E_{h\nu} > 6.2$ eV) for a typical cosmic ray ionization rate of $\xi \approx 10^{-17}$ s^{-1} (Sternberg et al. 1987; Gredel et al. 1989). The penetrating UV field intensity is dependent on position in the cloud as well as cloud morphology and will dominate over all other sources of UV photons in the outer cloud regions. The penetrating UV intensity in outer cloud regions has been estimated at $\sim 8 \times 10^7$ photons cm^{-2} s^{-1} ($E_{h\nu} > 6$ eV; Mathis et al. 1983).

The irradiation ratio R is adopted here as a measure of UV dose for convenient comparison between the expected processing of interstellar ice and the results of simulation experiments.

Send offprint requests to: W.A. Schutte

R is defined as the total amount of UV photons absorbed per solid H_2O molecule during a given time period and is calculated assuming an average H_2O UV cross-section of 2×10^{-18} cm^2 ($E_{h\nu} > 6$ eV; Okabe 1978). For example, $R = 0.06$ for a UV flux of $\sim$ 1000 photons cm^{-2} s^{-1} after 10^6 years.

The interstellar ice feature at 4.615 μm in the spectra of several embedded protostellar sources provides observational evidence for the UV photolysis of ice mantles in dense clouds (Lacy et al. 1984; Tegler et al. 1995). This band is well reproduced by the irradiation of laboratory ices which contain NH_3 and CO in an H_2O-dominated mixture and has been assigned to the OCN^- ion in previous experiments (Grim & Greenberg 1987). However, the species responsible for the interstellar feature is still uncertain (isonitriles such as CH_3NC also produce a good fit; see Grim & Greenberg 1987). Recent observations of embedded protostars and background field stars (Tegler et al. 1995) seem to indicate that this feature is confined to regions of early star formation. Taken together, these two facts point to an important role of such regions in the chemical processing of interstellar ices. It should also be noted here that UV photolysis does not only create new molecules in this way but may also destroy species already accreted onto an icy grain mantle.

There are a number of other astrochemical phenomena which may rely on UV irradiation in the interstellar medium. For instance, the solid organic materials observed in both the diffuse ISM and in cometary dust (Sandford et al. 1991; Pendleton et al. 1994; Kissel & Krueger 1987) may originate in the energetic processing of ice mantles in dense clouds (Greenberg & Yencha 1973). This connection has been supported by laboratory simulations which show the formation of complex organic species from initially simple ices by such processes (Agarwal et al. 1985; Briggs et al. 1992; Strazulla & Baratta 1992).

This paper is the first in a series of laboratory studies in which we describe the photochemical behavior of interstellar analogs by means of in-situ infrared spectroscopy. Such studies are important for a number of reasons. First, they will help to understand the composition of interstellar ices. Interpretation of future observations with the Infrared Space Observatory (ISO) in wavelength regions obscured from ground-based observers (e.g., the 5 - 8 μm region) call for high-quality laboratory data. Secondly, UV photolysis of icy grain mantles may also play an important role in the modification of the gas phase, since molecules are cycled through both phases as a result of accretion and desorption mechanisms (Blake et al. 1987; Brown & Charnley 1990; Millar et al. 1991; Charnley et al. 1992; Shalabiea & Greenberg 1994). Indeed, the incorporation of ice mantle photochemistry into models of dense interstellar clouds requires a quantitative analysis of laboratory analogs.

Previous studies of the UV properties of interstellar ice analogs have dealt mainly with mixtures of two or more ices (e.g., Hagen et al. 1979; Grim et al. 1989). This paper presents the results of UV photolysis experiments on pure ice samples of 9 molecules known or suspected to be important components of interstellar ice: H_2O, NH_3, CH_4, O_2, N_2, CO, CO_2, H_2CO, and CH_3OH. Understanding these simple systems is essential before confronting the photochemistry of more complex ices (to be presented in future papers). Moreover, detailed analyses of interstellar ice features have shown that ice mantles are not strictly homogeneous, and certain components exist in relatively pure states (Sandford et al. 1988; Tielens et al. 1991; Skinner et al. 1992; Schutte et al. 1996).

This paper is structured as follows. In Sect. 2 we describe the experimental equipment and procedures. Our results are presented in Sect. 3, and the photochemical reaction schemes are considered in Sect. 4. The astrophysical implications of this research are discussed in Sect. 5. Cross-sections for destruction by ultraviolet photons (crucial parameters in gas-grain chemical models) are determined from our data, along with the rates of formation for first-order products.

2. Experimental

2.1. Vacuum set-up and equipment

Ice samples were created inside a vacuum-manifold system which has been described previously in detail by Gerakines et al. (1995). The molecules to be studied were condensed onto a cold (10 K) CsI substrate positioned inside the sample chamber of a Fourier-transform infrared spectrometer (Bio-Rad FTS40a). The substrate may be rotated between two positions without breaking the vacuum, enabling deposition of subject gases, UV irradiation, and infrared spectroscopy to be performed. The temperature of the substrate is continuously adjustable between 10 K and room temperature using a resistive heater element.

A microwave discharge hydrogen flow lamp (Opthos instruments) was used to irradiate the ice samples. The flux of the lamp at the substrate is $\sim 10^{15}$ photons cm^{-2} s^{-1} ($E_{h\nu} >$ 6 eV; Hagen 1982; Weber & Greenberg 1985) and its spectrum is dominated by five bands centered at 1220 (Lyman-α), 1360, 1450, 1600, and 2800 Å(see Jenniskens et al. 1993). The lamp is mounted directly onto the sample chamber, and its UV flux is transmitted through a window of MgF_2, which is transparent to wavelengths greater than $\sim$ 1100 Å. The operating pressure of the lamp in these experiments was 0.6 mbar.

2.2. Ice samples

Deposited samples were $\sim$ 0.1 μm in thickness. Such thin layers ensure that all ice samples are optically thin throughout the wavelength range of the processing ultraviolet radiation (1100 to 3000 Å; Okabe 1978). These ices were deposited with flow rates between about $2 - 5 \times 10^{15}$ molec cm^{-2} s^{-1} (1 - 2 μm hr^{-1}) for 2.5 - 5 min.

As discussed in Gerakines et al. (1995), the metal walls of our system constantly produce residual gases which are impossible to remove entirely. The major constituent of this residual gas is H_2O ($\sim$ 90 %). The background condensation rate determined by IR spectroscopy was $\sim 3 \times 10^{12}$ molec cm^{-2} s^{-1} (3×10^{-3} μm hr^{-1}). The contamination level of the samples was therefore $\sim$ 0.1 - 0.2 %. At this rate, residual gases collecting on top of the sample ice become optically thick to the UV radiation after 28 hr (assuming $< \sigma_{UV}(H_2O) > = 2 \times 10^{-18}$ cm^2; Okabe 1978).

In order to isolate the ice sample from the background molecules condensing before and after sample deposition, the sample was deposited between two layers of argon. This procedure was made possible because of the two independent deposition systems of our setup (see Gerakines et al. 1995 for a complete description), with which the transition from sample to Ar depositions could be made nearly instantaneous. Some small overlap occurs, however, and is seen as features of Ar-isolated H_2O and NH_3 in the deposition spectra of these molecules.

Rare gas matrices (such as argon) are transparent to the UV radiation used to process the ice samples, since the energy range lies well outside their continuum or discrete electronic transition regions (Klein & Venables 1976), and so no attenuation is expected due to the layers of argon. Each argon layer was approximately 3 - 5 times the thickness of the sample ice ($\sim$ 0.3 - 0.5 μm). The deposition of each of the Ar layers was made at a rate of $\sim$ 2.4 $\times$ 10^{15} molec cm^{-2} s^{-1} ($\sim$ 3.5 μm hr^{-1}) for 10 min.

In order to determine the effects of the background species which became mixed with the sample, two experiments were performed for each molecule studied, using deposition rates which differed by about a factor of two. Thus, the number of products due to contaminations mixed with the sample molecule should change by approximately the same factor between the two experiments.

A blank experiment was also performed in which a single layer of solid Ar was irradiated for 1 hr at 10 K. This experiment showed that some CO and CO_2 is always produced due, most likely, to the interaction of H_2O ice from background accretion with a thin layer of organic material covering the CsI substrate. Using the features present in this control experiment, many small features were ruled out as possible products of sample molecules.

Ices maintained at 10 K were irradiated stepwise for one hour, pausing to take a spectrum at every step. The total irradiation time at each step was 5 s, 15 s, 1 min, 3 min, 10 min, and 1 hr, corresponding to UV doses of $R \approx 0.01$, 0.03, 0.12, 0.36, 1.2, and 7.2, respectively. These levels of irradiation therefore span the range of exposures expected for ice mantles in the dense ISM (see Sect. 1). After irradiation, samples were heated at $\sim$ 2 K min^{-1} to temperatures of $\sim$ 30, 60, 115, 150, 270 K, and a spectrum taken at each step.

When producing ice samples of IR inactive molecules such as Ar, N_2, and O_2, it is impossible to spectroscopically derive the quantity of gas deposited. To overcome this, we made depositions of an identical amount of sample molecule with a trace of CO. Since the strength of the CO 2138 cm^{-1} band in various ices is well known (e.g., Gerakines et al. 1995), the deposited CO abundance could be determined and used together with the mixing ratio to estimate the quantity of IR inactive molecules. This result was then used to calibrate the pressure increase (ΔP) needed at room temperature to set the deposition flow (see Gerakines et al. 1995). Inaccuracies in the mixing ratio and in the reproducibility of the flow at a given ΔP setting produce an error in the estimation of the deposited quantity of IR inactive molecules of about a factor of 2.

The reproducibility of the flux of the UV lamp was checked by comparisons of several experiments involving the same molecule. As an illustration, in the two 1 hr irradiations of solid H_2CO at 10 K, the percentage of H_2CO molecules destroyed differed by less than 1 % (the fraction of H_2CO remaining relative to the inital amount deposited equaled 6.5 and 5.8 %).

3. Results

In this section, we present the results of 9 ultraviolet photolysis experiments of pure ice samples at 10 K: H_2O, NH_3, CH_4, O_2, N_2, CO, CO_2, H_2CO, and CH_3OH. The infrared features which appear in the spectra of these ices as a result of UV irradiation are listed in Tables 1, 2, 4, 6, 7, and 9. We identify these bands with molecular features from the literature on the basis of a number of criteria. Since in most cases, literature data refer to measurements of ices isolated in different matrices (e.g., Ar or N_2), our first criterion is that the observed frequency should fall within 0.5 % of the listed position. Matrix shifts of this magnitude are often observed (Sandford et al. 1988; Sandford & Allamandola 1990; Schutte et al. 1996; Ehrenfreund et al. 1996). Secondly, we require that all strong bands which fall in relatively unobscured regions must be visible. Finally, the warm-up behavior should be consistent with the proposed assignment, and highly volatile or reactive species should disappear at relatively low temperatures. When all the above criteria are not obviously met, we will not explicitly identify such a feature, but enter it in our listings as "unidentified".

Species are designated as first or higher-order products of the photolysis, based on the initial growth rates of their infrared features. Linear growth indicates a first-order product, and quadratic (or steeper) growth represents higher order. Photoproduction yields after 1 hr of UV exposure are given in Tables 3, 5, 8, and 10 for species whose absolute band intensities are known.

As a consequence of using two relatively thick layers of argon on either side of the sample ice, a sinusoidal wavelength dependence is observed in the baseline of obtained spectra (see, for example, Fig. 11). This is due to interference by directly transmitted photons and those which are scattered between the substrate and the vacuum interface of the sample. In addition to the sinusoidal structure, features appear in all experiments at $\sim$ 3275, 1670, and 750 cm^{-1}, due to the continuous background condensation of H_2O (see Sect. 2).

For each experiment, we show the growth as a function of time for a number of IR features, selected to give an overview of the production of the various new species (Figs. 1, 2, 3, 5, 7, 8, 10, and 12). These curves may be converted to abundance at any time using the band intensities listed in Tables 3, 5, 8, and 10.

3.1. H_2O

Frequencies and identifications of the new infrared features which appear upon photolysis of H_2O are given in Table 1. The evolution of the bands of H_2O and its photoproducts is

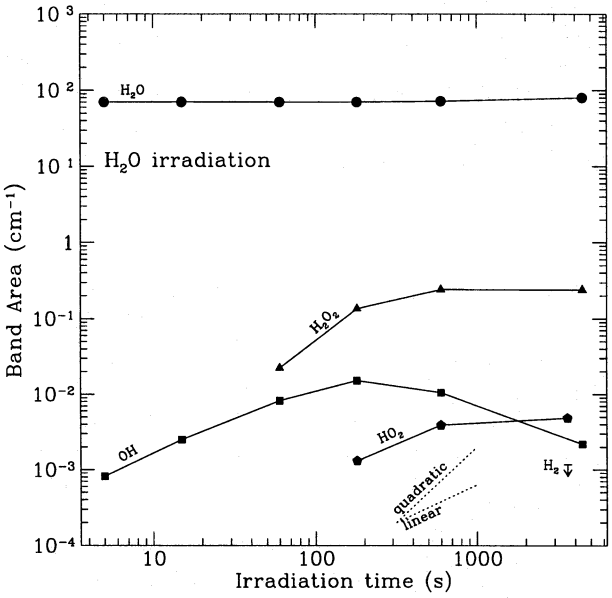

Fig. 1. Evolution of features in H_2O irradiation. H_2O is represented by its 3270 cm^{-1} band. All other bands are indicated in Table 1. The dotted lines indicate linear and quadratic time dependencies

Table 1. New bands observed during the photolysis experiments of solid H_2O and of solid NH_3 at 10 K. Product order is listed for bands whose evolution is displayed in Figs. 1 and 2

Ice studied	ν (cm^{-1})	Assignment	Order	Ref
H_2O	1101	HO_2		1
	1389[a]	HO_2	?	1
	1457	H_2O_2		2
	2850[a]	H_2O_2	≥ 2	2
	3413	HO_2		1
	3428	OH		3
	3453[a]	OH	1	3
	4143[a]	H_2		4
NH_3[b]	886	N_2H_4	?	5
	1505	NH_2	1	6
	2115	Unid.	1	
	4137	H_2		4

[a] Growth curve plotted in Fig. 1; [b] growth curves plotted in Fig. 2 for all listed features of NH_3 experiment.

References: 1 Jacox & Milligan 1972; 2 Giguère & Harvey 1959; 3 Acquista et al. 1968; 4 Sandford & Allamandola 1993; 5 Roux & Wood 1983; 6 Milligan & Jacox 1965.

shown in Fig. 1. OH, H_2O_2, and HO_2 have been identified as the main photoproducts of H_2O. The band of molecular hydrogen at 4143 cm^{-1} (Sandford & Allamandola 1993) was not clearly identified, but an upper limit on its production has been estimated.

Several properties of the features which appear at 3428 and 3453 cm^{-1} suggest that they are due to the OH radical. Both bands disappear between 30-70 K, indicating that they are due to a highly reactive species. Moreover, they grow simultaneously and display a similar warm-up behavior. Furthermore, these two features coincide with the doublet structure seen in Ar by Acquista et al. (1968) during the UV photolysis of Ar:H_2O mixtures with a ratio of 250:1. These authors conclude that this pattern most likely indicates OH radicals which reside in two distinctly different matrix sites: either isolated OH, or OH interacting with H_2O molecules. If a fraction of the sample and Ar depositions in our experiments overlap (see Sect. 2), or the layers penetrate each other to some extent during the photolysis, then an amount of H_2O molecules and their photoproducts may be isolated within the Ar layer to produce such a doublet effect. The growth of 3453 cm^{-1} band is plotted in Fig. 1 and shows a first-order time dependence, appearing after 5 s of UV exposure.

The features observed at 2850 and 1457 cm^{-1} are assigned to H_2O_2. After warm-up to 70 K, these bands have shifted to 2853 and to 1450 cm^{-1}, respectively. Giguère & Harvey (1959) have shown that bands due to H_2O_2 appear at 2840 and 1455 cm^{-1} in a crystalline mixture with H_2O at 80 K with a low H_2O_2 concentration (H_2O_2:$H_2O \sim 0.2$:1). These positions coincide by 0.5 and 0.3 % to the locations of the bands observed in these experiments. The 2850 cm^{-1} feature displays a second-order time dependence in Fig. 1 and is clearly seen after 1 min of photolysis.

The bands at 1101, 1389, and 3413 cm^{-1} are identified with the HO_2 ν_3, ν_2, and ν_1 fundamentals (Jacox & Milligan 1972). All bands disappear between 30 and 70 K.

3.2. NH_3

The features appearing during the photolysis of solid NH_3 at 10 K are listed with their identifications in Table 1. The evolution of selected features during photolysis is displayed in Fig. 2. Obvious products of the photolysis are N_2H_4 and NH_2, detected by the growth of features at 886 and 1505 cm^{-1}, respectively. A broad, strong band at 2115 cm^{-1} with a width of 90 cm^{-1}, which appears after only 15 s of UV photolysis, remains unidentified. This feature disappears after warm-up to 60 K, indicating a reactive species may be its carrier. There is no clear indication of diimide (N_2H_2) in our spectra at 1286, 1058, or 946 cm^{-1} (Rosengren & Pimentel 1965). Imidogen (NH) is also not seen at 3125 cm^{-1} (Rosengren & Pimentel 1965), possibly due to the strong NH_3 absorptions in this region.

3.3. CH_4

Numerous infrared features appear upon the photolysis of CH_4, suggesting a complex photochemistry (see Table 2). After only 5 s of irradiation, sharp features which may be ascribed to

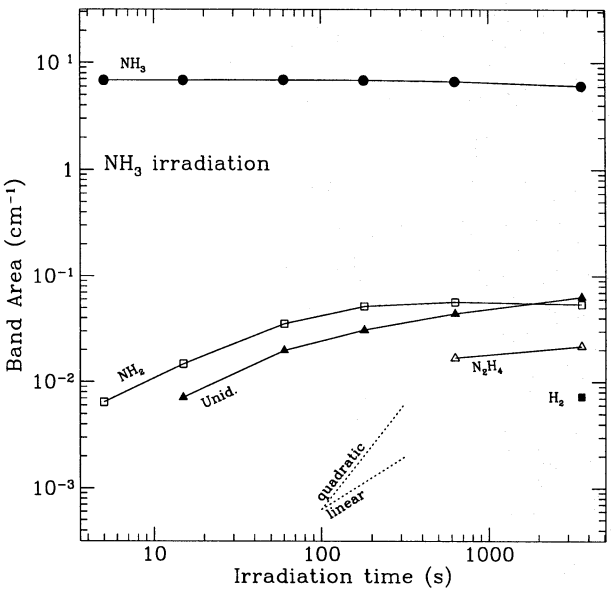

Fig. 2. Evolution of features in NH_3 irradiation. NH_3 is represented by its band at 1070 cm^{-1}. All other bands are indicated in Table 1. The dotted lines indicate linear and quadratic time dependencies

ethane (C_2H_6) occur at 822, 1375, 1465, 2882, 2908, 2942, and 2975 cm^{-1} (Comeford & Gould 1960). At larger doses, broader features grow underneath the sharp bands in the aliphatic C-H stretching region (3000 - 2800 cm^{-1}) and deformation region (1600-1200 cm^{-1}), indicating the formation of larger aliphatic structures. In particular, the growth of a feature at 750 cm^{-1} signifies the formation of propane (C_3H_8; Comeford & Gould 1960).

Besides the aliphatic features, relatively weak bands appear which may be assigned to unsaturated species (such as allene, ethylene, and carbon chains containing double and triple carbon bonds). However, no evidence is found for the presence of the smallest unsaturated species, acetylene (C_2H_2).

A feature at 608 cm^{-1} which disappears at low temperatures (30 K) suggests the presence of the CH_3 radical. There is no indication of the CH_2 radical, despite the fact that this species is a known product of the vacuum UV photolysis of gaseous methane (Okabe 1978).

No strong evidence for cyclic structures is found in our spectra. However, two unidentified bands at 738 and 950 cm^{-1} coincide with features generally produced by cyclic hydrocarbons with side chains (e.g., *n*-propylcyclohexane), substituted benzenes (e.g., toluene and xylene) and aromatics linked to chains, such as styrene (Aldrich Library).

Fig. 3 shows the integrated absorbances of selected infrared features of the detected species. Absorbance values for the C-H stretching region have been integrated over the entire frequency range (3000 - 2800 cm^{-1}) with the exclusion of the 3009 cm^{-1} CH_4 feature. The band area indicated in Fig. 3 is therefore indicative of higher aliphatics (ethane and larger). It may be seen

Table 2. New bands observed during the photolysis of solid CH_4 at 10 K. The full width at half-maximum (FWHM) is indicated for overlapping bands

ν (cm^{-1})	FWHM (cm^{-1})	Assignment	Comments	Ref
608[a]		CH_3		1,2
738		unid.		
750[a]		propane (C_3H_8)		3
822[b]		ethane (C_2H_6)		3
911[a]		$R_2C{=}CH_2$	δCH (out-of-plane)	4
950		unid.		
1235		unid.		
1375		R-CH_3	δ_sCH	
1375		ethane		3
1438	6	ethylene (C_2H_4)		3
1438	26	$R_2C{=}CH_2$	δCH in-plane	
1460		R-CH_3	δ_{as}CH	
1465	7	ethane		3
1470		R-CH_2-R	CH_2 scissor	
1645		R$_2$C=CHR	ν(C=C)	
1960		allene ($H_2C{=}C{=}CH_2$)		5
2850	8	R-CH_2-R	ν_s(C-H)	
2875	15	R-CH_3	ν_s(C-H)	
2882	6	ethane		3
2908	5	ethane		3
2916	7	propane		3
2933	16	R-CH_2-R	ν_{as}(C-H)	
2942	11	ethane		3
2962	26	R-CH_3	ν_{as}(C-H)	3
2975[c]	11	ethane		3
3095[a]		ethylene		3,6,7
3248		H-C≡C-R	ν(C-H)	8
3270		H-C≡C-R	ν(C-H)	8
3315[a]		H-C≡C-R	ν(C-H)	4,9

[a] Growth curve plotted in Fig. 3; [b] used for growth curve in later timesteps; [c] used for growth curve in early timesteps.

References: 1 Pacansky & Bargon 1975; 2 Pacansky et al. 1981; 3 Comeford & Gould 1960; 4 Aldrich Library; 5 Seloudoux et al. 1979; 6 Duncan et al. 1973; 7 Brecher & Halford 1961; 8 Saussey et al. 1976; 9 Maki & Toth 1965.

that even after the growths of ethane (first) and propane (second) have leveled off, the integrated absorption of the C-H stretching region continues to increase due to the production of even larger aliphatics, reflecting an increasing molecular complexity with UV dose.

In Table 3, the derived abundances for the various species after 1 hr of UV photolysis are given. Spectroscopically, it is quite difficult to derive separate abundances for various hydrocarbons from overlapping C-H stretching modes. However, separate abundances for species of different volatilities may be estimated from the spectra obtained after warm-up to 115 and 290 K, since many molecules evaporate between 10 - 115 K and between 115 - 290 K. The sizes of these evaporating species

Table 3. Band intensities, A (in cm C atom^{-1}), and abundances after 1 hr UV irradiation at 10 K relative to the initial CH_4 abundance

Molecule	Band Position (cm^{-1})	A (cm C atom^{-1})	Ref	Rel to initial dep (%)
CH_4	3009	6.4(-18)	1	38
C_2H_6	3100-2800	6.5(-18)	2	8.0
higher-order volatiles[a]	3100-2800	6.5(-18)	2	9.0
higher-order residue[b]	3100-2800	6.5(-18)	2	14
C_2H_4	1438	8.5(-19)	3	2.6
CH_3	608	2.5(-17)	4	0.01
$H_2C{=}C{=}CH_2$	1960	2.6(-18)	5	0.6

[a] Between $\sim$ 2 and $\sim$ 7 C atoms; [b] at room temperature, number of C atoms $\geq$ 7.

References: 1 d'Hendecourt & Allamandola 1986; 2 Wexler 1967; 3 Fan & Ziegler 1992; 4 Wormhoudt & McCurdy 1989; 5 Youngquist et al. 1979.

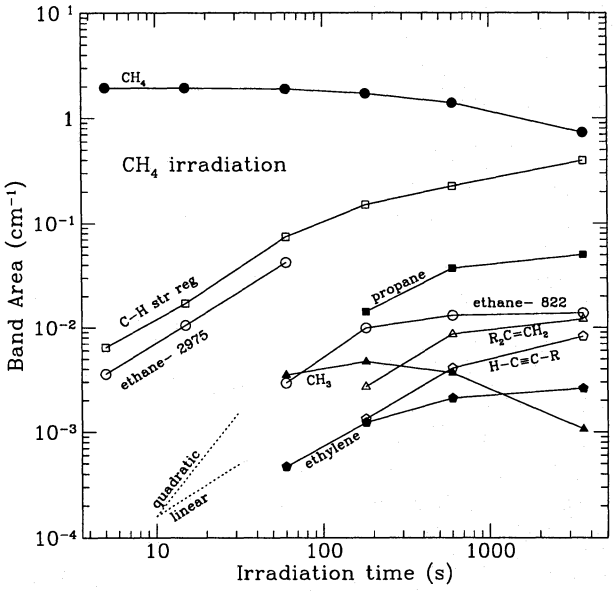

Fig. 3. Evolution of features in CH_4 irradiation. The growth of the entire C-H stretching region (3000 - 2800 cm^{-1}) is shown. CH_4 is represented by its 3009 cm^{-1} band. The 2975 cm^{-1} feature of ethane has been plotted in early time steps, when there is little overlap with broader structures. In later timesteps, the weaker 822 cm^{-1} band of ethane has been plotted. All other features are indicated in Table 2. The dotted lines indicate linear and quadratic time dependencies

may be roughly estimated by comparing the observed sublimation temperatures with those of molecules for which this value has been previously established under vacuum conditions: e.g., H_2CO (which sublimes at $\sim$ 115 K; Schutte et al. 1993), and the most volatile component of the room temperature organic residue obtained by the irradiation of ices under vacuum, hydroxyacetamide ($HOCH_2CONH_2$; Agarwal et al. 1985; Briggs et al. 1992).

The boiling point of a component should be a reasonable indicator of its sublimation behavior under vacuum. Comparing the boiling points of formaldehyde and hydroxyacetamide (252 and 393 K, respectively) with that of alkanes, we find that ethane should sublime below 115 K, but larger products should not. This is in good agreement with the observed behavior of the ethane and propane bands in these experiments (see Table 3). In the interval from 115 K to room temperature, all alkanes containing less than $\sim$ 7-8 C atoms should evaporate according to this criterion.

The final abundances listed in Table 3 indicate that 72 % of the carbon atoms after 1 hr of UV irradiation have been accounted for by the molecules identified. It should be pointed out that the mass density of amorphous solid CH_4 used to derive the band strengths of its infrared features is relatively uncertain and is generally assumed to be equal to that of H_2O for these purposes. Recent work suggests a much lower value, about 0.53 g cm^{-3} (Kaiser, private communication). The abundance of solid CH_4 deposited in these experiments is therefore equally as uncertain, and this fact may help to explain the apparent lack of carbon conservation observed here.

It is interesting to note that the ratio of CH_3:CH_2 groups indicated by the relative intensities of their ν_{as}(C-H) modes is as large as $\sim$ 2 at 115 K and $\sim$ 1 at room temperature. For linear alkane groups of the expected size range for these temperatures ($\geq$ 3 and $\geq$ 7 C atoms, respectively) this ratio should be much smaller. We conclude that the large alkanes produced in these experiments may contain highly branched structures.

Ausloos et al. (1965) have reported the results of the UV photolysis of an Ar:CH_4 = 40:1 mixture. Although they indicate the production of similar species to those presented here, the relative abundances of the larger species (butanes, pentanes, etc.) is much smaller in their experiments. This could perhaps

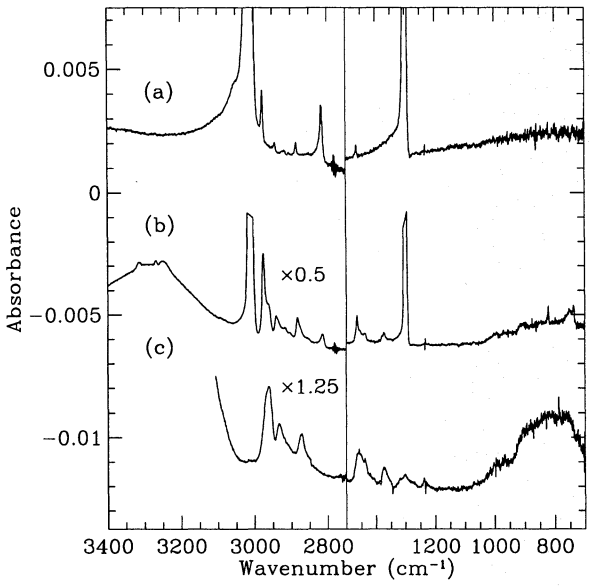

Fig. 4a–c. IR spectra of solid CH_4. *a* After 1 min UV irradiation at 10 K, bands of solid ethane are present at 2975, 2942, 1465, & 1375 cm^{-1}; *b* After 1 hr UV, many bands are present in both regions due to higher-order hydrocarbons; *c* At 115 K, ethane has evaporated, leaving the broad features due to larger alkanes and carbon chains. The 3009 and 1302 cm^{-1} bands of CH_4 have been truncated in *b* to accentuate smaller features. The 3300 cm^{-1} band of background H_2O has been truncated in *c*

be due to their Ar dilution, leading to less interactions between the photoproducts.

3.4. CO

Features appearing during the photolysis of solid CO at 10 K are listed in Table 4. Bands of CO_2, C_2O, C_3O, and C_3 have been observed. The bands of CO_2 appear at 660, 2347, 3602, and 3709 cm^{-1} (e.g., Hudgins et al. 1993 and references therein).

After long irradiation times (1 hr), the band we associate with C_3O at 2243 cm^{-1} becomes a sharp doubly-peaked structure, with a second peak falling at 2248 cm^{-1}. The growth of this second peak seems to correspond with a weak band centered near 2400 cm^{-1} in our spectra. We assign these bands to the carbon suboxide molecule, C_3O_2, in fair agreement with previously reported bands of this species at 2400 and 2255 cm^{-1} in Smith & Leroi (1966). However, this remains a tentative assignment, since other strong features of C_3O_2 were not seen near 1580 and 530 cm^{-1} (Smith & Leroi 1966).

CO_2 is produced by reactions of CO with the background H_2O as well as by reactions of CO molecules alone. Since two experiments with different contamination levels were performed (see Sect. 2), it is possible to derive and remove the excess CO_2 abundance from our measurements. The correction factor was found to be only 1 and 2 % of the original CO_2 abundances in the two experiments. CO_2 is also formed by reactions of background

Table 4. New bands observed during the photolysis of solid CO and of solid CO_2 at 10 K. Product order is listed for bands whose growth during irradiation is displayed in Figs. 5 and 7

Ice studied	ν (cm^{-1})	Assignment	Order	Ref
CO	660	CO_2		1
	1989	C_2O		2
	2028[a]	C_3	?	3
	2243[a]	C_3O	≥ 2	3
	2248	C_3O_2		4
	2281	$^{13}CO_2$		1
	2347[a]	CO_2	1	1
	2400	C_3O_2		4
	3413	Unid.		
	3550	Unid.		
	3602	CO_2		1
	3709	CO_2		1
CO_2	706	O_3		5
	976	CO_3		6
	1043[b]	O_3	≥ 2	5
	1053	Unid.		
	1067	CO_3		6
	1883	CO_3		6
	2044[b]	CO_3	1	6
	2093	^{13}CO		1
	2141[b]	CO	1	1
	2243[b]	C_3O	≥ 2	3

[a] Used for growth curve in Fig. 5; [b] used for growth curve in Fig. 7.

References: 1 Hudgins et al. 1993; 2 Jacox et al. 1965; 3 DeKock & Weltner 1971; 4 Smith & Leroi 1966; 5 Brewer & Wang 1972; 6 Moll et al. 1966.

Table 5. Band intensities (in cm $molec^{-1}$) and abundances after 1 hr UV at 10 K relative to the initial abundance for both the CO and CO_2 experiments

Ice	Product	Band Position (cm^{-1})	A (cm $molec^{-1}$)	Ref	Rel to initial dep (%)
CO	CO	2138	1.1(-17)	1	100
	CO_2	2342	7.6(-17)	1	0.8
CO_2	CO_2	2342	7.6(-17)	1	59
	CO	2138	1.1(-17)	1	32
	CO_3	2044	5.4(-18)[a]		9[a]
	O_3	1043	1.4(-17)	2	5.9

[a] Estimated assuming CO_3 contains all remaining C atoms.

References: 1 Gerakines et al. 1995; 2 Smith et al. 1985.

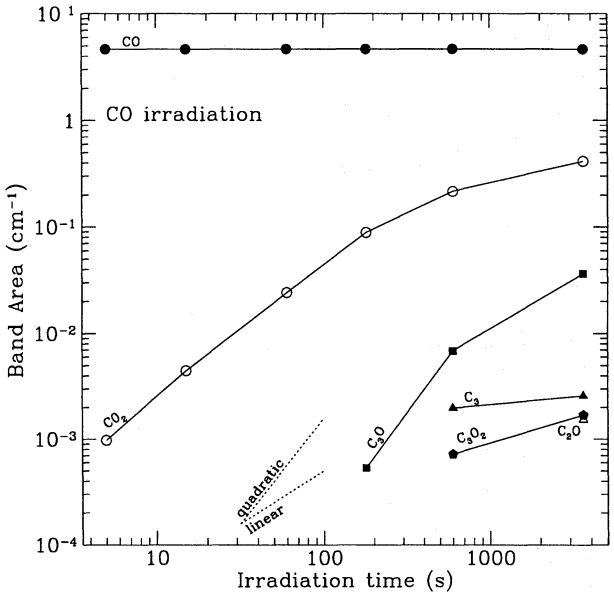

Fig. 5. Evolution of features in the CO irradiation. CO is represented by its stretching feature at 2138 cm^{-1}. All other features are indicated in Table 4. The dotted lines indicate linear and quadratic time dependencies

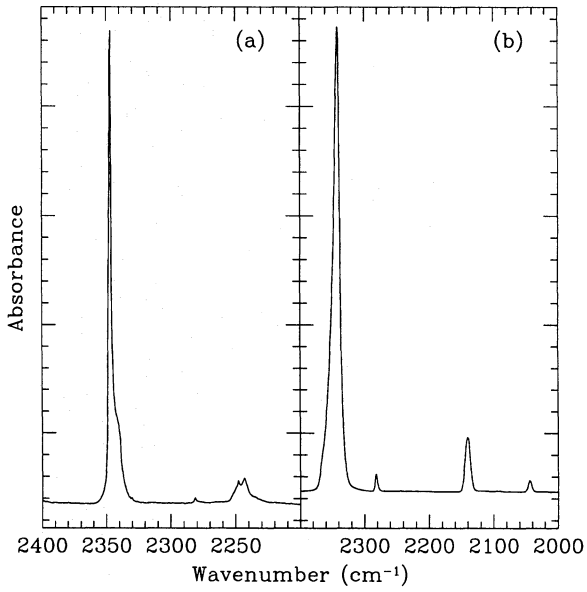

Fig. 6. *a* 2400 - 2200 cm^{-1} region of solid CO ice after 1 hr irradiation at 10 K. The C=O stretching features of CO_2 and $^{13}CO_2$ are present at 2342 and 2281 cm^{-1}, and the doubly-peaked structure of the C_3O and C_3O_2 bands may be seen at 2243 and 2248 cm^{-1}; *b* 2400 - 2000 cm^{-1} region in the spectrum of solid CO_2 ice after 1 hr of UV irradiation at 10 K. The features at 2342 and 2280 cm^{-1} are due to CO_2 and $^{13}CO_2$, respectively. Bands due to CO and CO_3 at 2138 and 2044 cm^{-1} are apparent

H_2O with organic material on the CsI substrate (see Sect. 2.2). This is removed from our measurements using results from the photolysis of a layer of pure Ar (descirbed in Sect. 2.2).

During warm-up, all observed species evaporate simultaneously with CO at T ≈ 30 K. No sign of any residue was found.

3.5. CO_2

A list of features appearing during the photolysis of solid CO_2 at 10 K is given in Table 4. The primary product is CO, given the short timescale in which the 2138 cm^{-1} band appears in our spectra. Two bands also appear at 706 and 1043 cm^{-1}, and are assigned to O_3. Upon warm up to 30 K, the 1043 cm^{-1} band increases in depth by 7 %, indicating that trapped O atoms are diffusing through the matrix to form more O_3 (Grim & d'Hendecourt 1986).

Estimated abundances of the photoproducts of CO_2 after 1 hr of UV irradiation are given in Table 5. Since the band intensities of the CO_3 features are not known, the final abundance of CO_3 and the intrinsic strength of its 2044 cm^{-1} band have been calculated assuming that all carbon atoms not tied up in CO and CO_2 are contained in the CO_3 molecules. Consequently, under this assumption 97 % of available oxygen atoms are accounted for in CO_2, CO, CO_3, and O_3, although a certain quantity is expected to be bound in O_2 as well. All bands due to the CO_2 photolysis have disappeared at 115 K, with no residue remaining.

Table 6. New bands observed during the photolysis of solid O_2 and of solid N_2 at 10 K

Ice studied	ν (cm^{-1})	Assignment	Ref
N_2	2150[a]	N_3	1
O_2	705	O_3	2
	1040	O_3	2
	1105	O_3	2
	1550	O_2	3,4
	1720	O_3	2
	2046	O_3	2
	2110	O_3	2
	3030	O_3	2

[a] Tentative assignment, appears as a shoulder on contamination CO feature.

References: 1 Milligan et al. 1956; 2 Brewer & Wang 1972; 3 Cairns & Pimentel 1965; 4 Ehrenfreund et al. 1992.

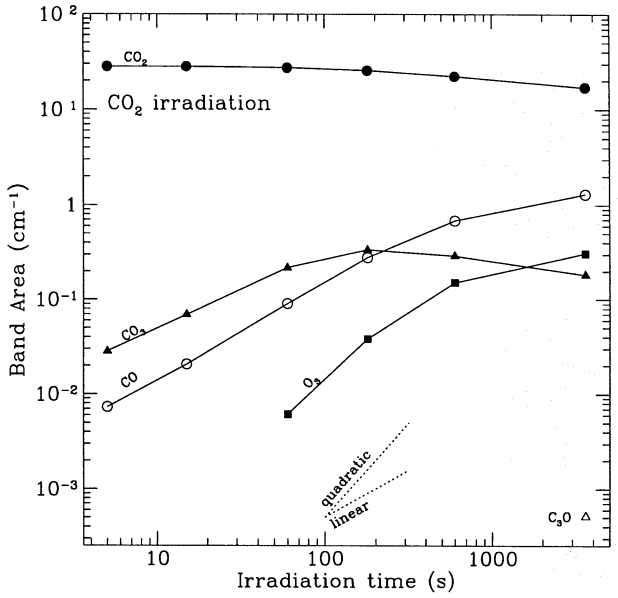

Fig. 7. Evolution of features in CO_2 irradiation. CO_2 is represented by its band at 2342 cm^{-1}. All other features are indicated in Table 4. The dotted lines indicate linear and quadratic time dependencies

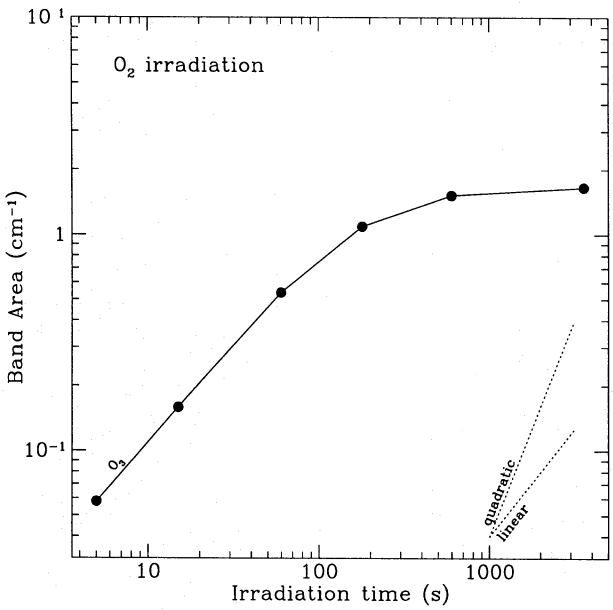

Fig. 8. Evolution of the strong ν_3 feature of O_3 (1043 cm^{-1}) in the O_2 irradiation. The dotted lines indicate linear and quadratic time dependencies

3.6. N_2

N_3, which is the only expected photolysis product of molecular nitrogen, has been reported to have an asymmetric stretching feature falling at 2150 cm^{-1} (Milligan et al. 1956). This band was not seen in these experiments since it unfortunately overlaps with the feature of CO produced by reactions of contamination molecules impossible to remove entirely (see Sect. 2.2). A strong shoulder on this band was seen, however, and falls at the correct location (2150 cm^{-1}). A contribution to this shoulder is most likely due to the CO satellite band located at this frequency (Sandford et al. 1988). Upon warm-up of the ice matrix, however, the shoulder observed here increases in strength relative to its neighboring CO contamination feature. We make a tentative assertion that part of this shoulder may be due to the band of N_3, since it appears in this strength only in the experiments involving N_2. No other features due to products of N_2 photolysis were observed.

3.7. O_2

The UV irradiation of molecular oxygen leads quickly to the production of ozone (O_3), which was observed as the solitary photolysis product in these experiments (see Table 6).

The matrix-induced 1550 cm^{-1} band of molecular oxygen appears in our spectra after 1 min of UV irradiation. Although O_2 is a homonuclear diatomic species which is usually IR inactive, this molecule has been shown to absorb weakly at this frequency when situated in a matrix of molecules with which it may interact (Cairns & Pimentel 1965; Ehrenfreund et al. 1992).

The abundance of deposited O_2 has been estimated using the method described in Sect. 2.2. The abundance of ozone produced was calculated using the gas-phase value for the band strength of the 1040 cm^{-1} ν_3 fundamental, 1.4×10^{-17} cm $molec^{-1}$ (Smith et al. 1985). Hence, we have derived that 36 % of the initially deposited O_2 was converted to O_3 after 1 hr of UV irradiation at 10 K.

3.8. H_2CO

Fig. 9 shows the unirradiated H_2CO sample at 10 K, the same ice after 1 hr of UV photolysis, and again after warm-up to 190 K. Many new features appear upon photolysis, and the irradiated spectrum bears little similarity to that of the pure ice. The ice spectrum after warm-up to 190 K shows strong residual features, suggesting the presence of highly refractory species. Positions and identifications of new features at listed in Table 7. The main initial product is the formaldehyde polymer polyoxymethylene (POM), with relatively small yields of CO and HCO. Derived abundances for assigned species after 1 hr of photolysis are given in Table 8.

The CO band continued to grow during the entire irradiation period, even after almost all H_2CO had been consumed by the photolysis. This indicates an additional source of CO: presumably the POM chains produced in high abundances in later irradiation stages.

The 1723 cm^{-1} feature is assigned to the aldehyde C=O stretching mode–the terminal group of POM chains. Methyl formate (H_3COHCO), the smallest product of H_2CO polymerization, may also contribute to this feature. The presence of methyl formate was confirmed by a second feature at 1161 cm^{-1} in our

Table 7. New bands observed during the photolysis of solid H_2CO at 10 K. Product order is given for bands whose evolution is displayed in Fig. 10

ν (cm^{-1})	Assignment	Order	Ref
627	POM ($HCO[CH_2O]_nH_2COH$)		1
656	CO_2		2
944	POM		1
993	POM		1
1030[a]	CH_3OH	≥ 2	2
1071	C-OH; ν(C-O)		3
1110[a]	POM	1	1
1161	H_3COHCO; ν(C-O)		3
1223	POM		1
1283	unid.		
1304[a]	CH_4	≥ 2	2
1351	unid.		
1381	POM		1
1428	POM		1
1440	$HCO[HCOH]_nH_2COH$; δ(C-H)		3
1468	POM		1
1722[a]	H_3COHCO, POM endgroups; ν(C=O)	≥ 2	1
1844[b]	HCO	1	4
1863[b]	HCO	1	5
2090	^{13}CO		2
2138[a]	CO	1	2
2244	C_3O		6
2277	$^{13}CO_2$		2
2342[a]	CO_2	≥ 2	2
2911	POM		1
3300	$HCO[HCOH]_nH_2COH$; ν(O-H)		3
4140[a]	H_2		7

[a] Growth curve shown in Fig. 10; [b] combination of 1844 and 1863 cm^{-1} bands used for growth curve.

References: 1 Schutte et al. 1993; 2 Hudgins et al. 1993; 3 Aldrich Library; 4 Schutte 1988; 5 Milligan & Jacox 1971; 6 DeKock & Weltner 1971; 7 Sandford & Allamandola 1993.

Table 8. Derived final abundances after 1 hr of UV irradiation at 10 K relative to the initial H_2CO abundance

Product	Band Position (cm^{-1})	A (cm $molec^{-1}$)	Ref	Rel to initial dep (%)
POM	937	3.0(-17)[a]	1	33[a]
CO	2138	1.1(-17)	2	15
$HCO[HCOH]_nH_2COH$	3300	4.2(-17)[a]	3	11[a]
C=O end groups	1720	2.3(-17)[a]	3	6.9[a]
H_2CO	1494	3.9(-18)	1	5.8
CO_2	2342	7.6(-17)	2	2.1
CH_3OH	1026	1.8(-17)	4	1.5
CH_4	1302	6.1(-18)	4	0.7
HCO	1863	1.0(-17)[b]		0.01

[a] per C atom; [b] assumed for HCO.

References: 1 Schutte et al. 1993; 2 Gerakines et al. 1995; 3 Wexler 1967; 4 d'Hendecourt & Allamandola 1986; 5 Sandford & Allamandola 1993.

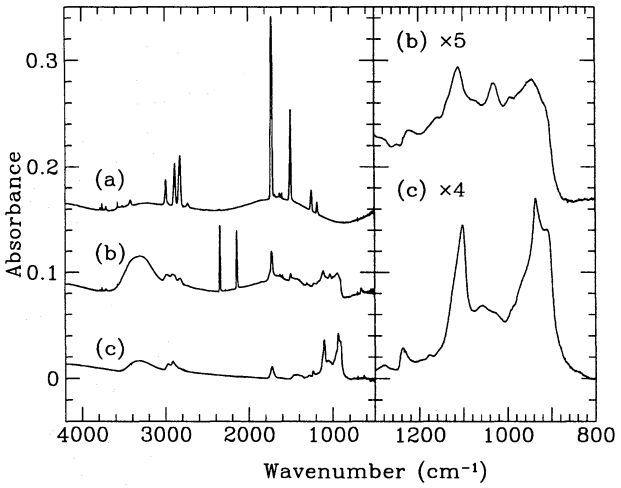

Fig. 9. Spectrum of H_2CO ice: (a) at 10 K after deposition; *b* at 10 K after 1 hr UV irradiation; *c* after 1 hr irradiation and warm-up to 190 K. Enlargements of curves *b* and *c* are given in the 1300 - 800 cm^{-1} region to clearly display the features due to H_2CO polymers (POM). Sinusoidal baseline behavior is due to scattering in the two Ar layers (see Sect. 3 above)

spectra, close to the position of the C-O stretching mode of the ester group (-C-O-HCO). The 1161 cm^{-1} feature disappeared between 115 - 190 K, indicating that its carrier is a molecule with approximately the same volatility as CH_3OH, consistent with the proposed assignment.

Features at 1844 and 1863 cm^{-1} are attributed to solid HCO in two different sites in the matrix. These features show the same initial growth during irradiation and the same warm-up behavior, although the band at 1844 cm^{-1} became relatively weaker after 1 hr of photolysis. The position of the 1863 cm^{-1} band coincides with the band of HCO seen by Hagen (1982 and references therein) in ice matrices dominated by CO, while the 1844 cm^{-1} feature is close is position to the band of HCO observed by Schutte (1988) in mixtures with H_2O. Hence, the areas of both features have been combined to give the growth curve seen in Fig. 10.

After warm-up to 190 K (after background H_2O evaporation, see Sect. 2), the spectrum is dominated by the features of POM. A strong band centered at 3300 cm^{-1} is also observed, presumably due to the O-H stretch of $HCO[HCOH]_nH_2COH$ polymers. Such structures are well-known polymerization products of H_2CO (Walker 1964). It should be noted, however, that no features were found which could be attributed to glycoaldehyde (CH_2OHHCO; Sodeau & Lee 1978). Thus, these polymers

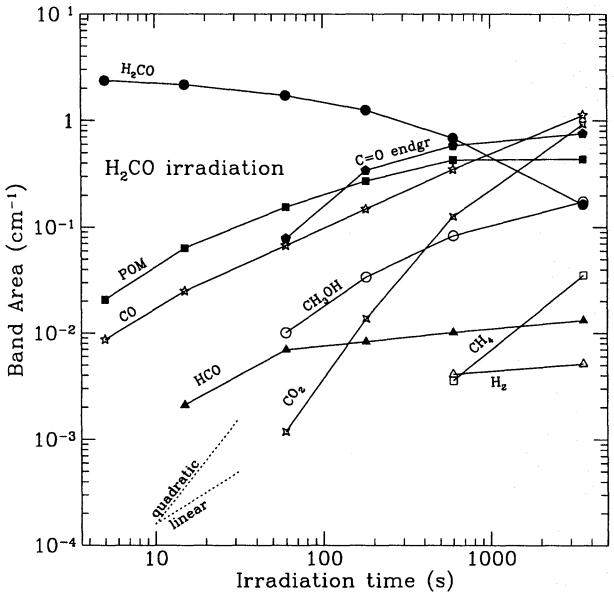

Fig. 10. Evolution of features in H_2CO irradiation. H_2CO is represented by its 1494 cm^{-1} feature. All other bands are indicated in Table 7. The dotted lines indicate linear and quadratic time dependencies

should contain as least 3 carbon atoms (e.g., glyceraldehyde $HOCH_2HCOHHCO$). Glyceraldehyde has been proposed as a possible precursor of the organic residues produced by irradiating ices containing H_2O, CO, and NH_3 (Agarwal et al. 1985, Briggs et al. 1992; Schutte 1988).

Band strengths and relative abundances of final products of the H_2CO irradiation are listed in Table 8. The listed abundances account for 76.1 and 78.2 % of initial carbon and oxygen atoms, respectively. This discrepancy may be accounted for by uncertain or unknown band strengths (or to some extent by the molecules producing the unidentified features in our spectra), since the band strengths for some molecules may be uncertain by a factor of 1.5 - 2 (see discussion in Boogert et al. 1996).

3.9. CH_3OH

Fig. 11 displays the spectrum of solid CH_3OH at 10 K just after deposition, along with the spectrum following 1 min and 1 hr of UV photolysis. Many new features are evident, indicating a complex photochemistry for methanol. Features appearing in the photolysis of solid CH_3OH at 10 K are listed in Table 9. The evolution of selected bands during photolysis is shown in Fig. 12.

The band listed at 1718 cm^{-1} appeared as a broad component underneath the sharper band of H_2CO at later stages of the photolysis. In the H_2CO irradiation (previous section), we assigned this feature both to the aldehyde endgroups on POM chains and to methyl formate (H_3COHCO), but since no POM was observed during the CH_3OH photolysis, we assign the band exclusively to methyl formate. The presence of this species is also indicated by the appearance of a feature at 1160 cm^{-1}

Table 9. New bands observed during the photolysis of solid CH_3OH at 10 K. Product order is listed for bands whose evolution is displayed in Fig. 12

ν (cm^{-1})	Assignment	Order	Ref
655	CO_2		1
910	H_3COHCO		2
1088	C-OH stretch (alcohols)		3
1160	H_3COHCO; ν(C-O)		3
1197	CH_2OH		4
1244[a]	H_2CO	1	2
1304[a]	CH_4	1	1
1352	CH_2OH		4
1497	H_2CO		2
1718[a]	H_3COHCO	≥ 2	2
1719	H_2CO		2
1850[b]	HCO	?	5
1863[b]	HCO	?	6
2092	^{13}CO		1
2138[a]	CO	≥ 2	1
2278	$^{13}CO_2$		1
2342[a]	CO_2	≥ 2	1
3011	CH_4		1
4140[a]	H_2		7

[a] Growth curve shown in Fig. 12; [b] combination of 1850 and 1863 cm^{-1} bands used for growth curve.

Refs: 1 Hudgins et al. 1993; 2 Schutte et al. 1993; 3 Aldrich Library; 4 Jacox 1981; 5 Schutte 1988; 6 Milligan & Jacox 1971; 7 Sandford & Allamandola 1993.

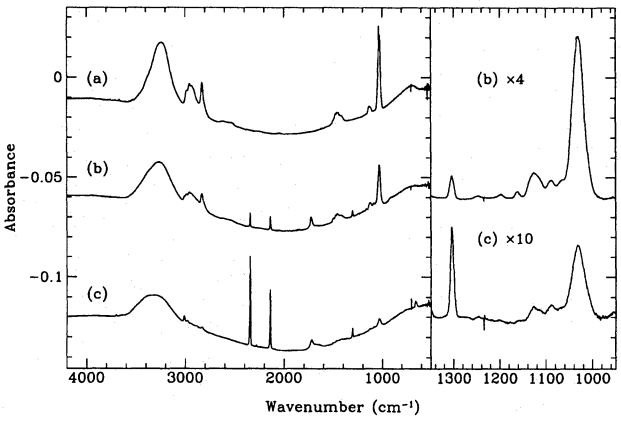

Fig. 11. Spectrum of solid CH_3OH ice at 10 K: (a) after deposition; *b* after 10 min UV photolysis– bands due to first-order products are seen; *c* after 1 hr UV irradiation. The region from 1350 - 950 cm^{-1} of spectra *b* and *c* are enlarged for comparison. The sinusoidal baseline behavior is due to scattering in the two Ar layers (see Sect. 3 above)

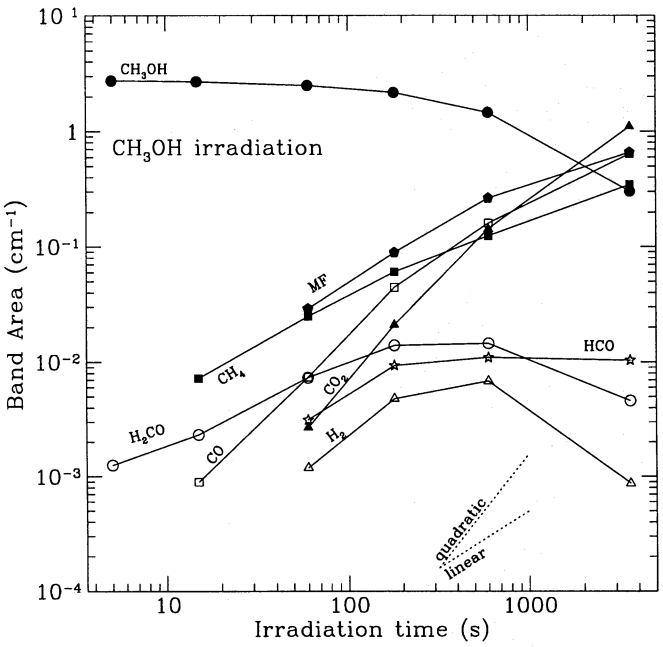

Fig. 12. Evolution of features in CH_3OH irradiation. CH_3OH is represented by its 1026 cm^{-1} band. All other features are indicated in Table 9. MF = methyl formate. The dotted lines indicate linear and quadratic time dependencies

Table 10. Abundances after 1 hr of UV irradiation at 10 K relative to the initial CH_3OH abundance

Molecule	Band Position (cm^{-1})	A (cm $molec^{-1}$)	Ref	Rel to initial dep (%)
CO	2138	1.1(-17)	1	39
H_3COHCO	1718	1.2(-17)	2	13
CH_3OH	1026	1.8(-17)	3	11
CO_2	2342	7.6(-17)	1	9.3
CH_4	1302	6.1(-18)	3	8.0
HCO	1863	1.0(-17)[a]		0.67
H_2CO	1494	3.9(-18)	4	3.0
H_2	4140	$\geq$ 9(-20)	5	$\leq$ 5.9

[a] Assumed for HCO.

References: 1 Gerakines et al. 1995; 2 Wexler 1967; 3 d'Hendecourt & Allamandola 1986; 4 Schutte et al. 1993; 5 Sandford & Allamandola 1993.

(identical to the band observed in the H_2CO irradiation ascribed to the methyl formate ν(C-O) mode) as well as a weak third feature at 910 cm^{-1}. Clearly, rather than forming large polymers (as obtained in the photolysis of pure H_2CO, Sect. 3.8), the H_2CO produced by the CH_3OH photolysis is converted to relatively small products. This is most likely related to its low concentration in the ice matrix (< 8 % at any stage of the experiment). From Table 10, it may be seen that after CO, methyl formate was the most abundant product at long irradiation times.

The features which appeared at 1850 and 1863 cm^{-1} have each been attributed to the radical HCO. Both features appear simultaneously, show the same warm-up behavior, and are gone at 60 K. As observed in the H_2CO photolysis, the appearance of two bands of HCO near 1860 cm^{-1} seems to indicate that this species resides in two distinctly different matrix sites (see previous section). In this experiment, the 1850 cm^{-1} band was only $\sim$ 2 times stronger than the 1863 cm^{-1} feature, and the relative strengths of these features remained almost constant throughout the irradiation. As in the H_2CO experiment, the sum of the 1850 and 1863 cm^{-1} absorptions has been used to monitor the HCO time dependence, and is shown in Fig. 12.

Higher-order alcohols such as ethanol (C_2H_5OH) and ethylene glycol ($HOCH_2CH_2OH$) typically display a feature near 1085 cm^{-1} (Aldrich Library), and therefore may be responsible for the band at 1088 cm^{-1} observed in these experiments. However, a second feature of approximately the same strength near 880 cm^{-1} which is also associated with these species is not observed. The observed 1088 cm^{-1} band disappeared between 120 and 230 K, indicating a carrier with about the same volatility as methanol.

Features observed at 1197 and 1352 cm^{-1} coincide reasonably well (within $\sim$ 1 %) with the reported bands of the CH_2OH radical at 1183, and 1334 cm^{-1} produced in the irradiation of Ar:CH_3OH = 200:1 mixtures (Jacox 1981). The methoxy radical (CH_3O) could not be detected in our experiments, since its features near 1040 and 2820 cm^{-1} (Chesters & McCash 1987) overlap with strong methanol bands.

3.10. UV destruction cross-sections

The initial photodestruction of a species in an optically thin sample is given by

$$N(t) = N(0)\exp(-\phi \cdot t \cdot \sigma_{\rm des}) \quad (1)$$

where N is the abundance of the species (in cm^{-2}), $N(0)$ is the initial abundance, $\sigma_{\rm des}$ is the cross-section for destruction by photolysis (in cm^2), ϕ is the flux of UV photons (in photons cm^{-2} s^{-1}), and t is the irradiation time (in s). It must be noted that $\sigma_{\rm des}$ does not only depend on the photodissociation of the species, but also reflects the possibility that the molecule may react with a hot product of the photolysis.

As an example of the validity of Eq. 1, Fig. 13 shows a semi-log plot of CH_4 abundance vs. time. Initially, the rate of destruction has an exponential behavior. In later times, however, it can be seen that the destruction falls below an exponential rate. This is a general property of all of our experiments, which is primarily caused by the re-formation of the original species from its photoproducts. Changes in the optical properties of the ice sample may change the UV penetration and add to this effect as well.

In general, we have fit the first five points (at t = 0, 5 s, 15 s, 1 min & 3 min) of log(N) vs. t to derive a value for the destruction cross-section, $\sigma_{\rm des}$. For H_2CO, only the first four points were used, since its destruction rate already loses its exponential character after 1 min. In some cases, however, this proce-

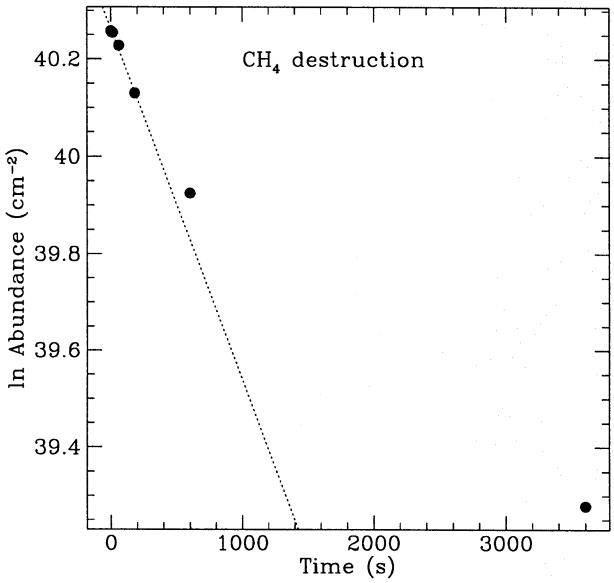

Fig. 13. Semi-log plot demonstrating the method for determining destruction cross-sections, σ_{des}, which is given by the slope of a linear fit to the points at t = 0, 5, 15, 60, and 180 s

dure was not feasible. For H_2O, problems arose due to constant deposition of background gases and hydrogen bond formation between initially isolated H_2O molecules (see Sect. 2). For the experiments with ammonia, NH_3 molecules initially isolated in the Ar layer created a similar difficulty. In the CO irradiations, the CO feature does not appear to weaken, even for timesteps of about 1 hr. Therefore, we may only estimate an upper limit for its destruction cross-section. We have indirectly calculated the O_2 column density as a function of time based on the observed O_3 abundance, and could therefore determine σ_{des} as for the other species.

In a number of cases the destruction is only partially caused by direct photon absorption, and reactions with photoproducts also make a major contribution. In the case of O_2, the cross-section for destruction due solely to photodissociation may be about one-third of the observed total destruction cross-section, since each O atom produced has a high probability to from O_3 by reaction with a neighboring O_2 molecule. Similar processes will enhance the destruction rates of the other species, with the possible exception of CH_3OH (see Sect. 3.9). Thus, it appears likely that the destruction cross-sections will show considerable dependences on the ice environment and could differ significantly if the species resides in mixtures with other molecules. In any case, Table 11 gives a number of base values which may be used for comparison and for understanding the results obtained for more complex ices.

It can be seen from Table 11 that there is a large variation in the destruction cross-sections for the molecules studied here. By far the most susceptible species to UV in these experiments is H_2CO, which is related to its very efficient polymerization. Although the photodestruction of H_2O and NH_3 could not be measured directly, the lack of abundant products in the photolysis of these molecules (Sect. 3.1 and 3.2) suggests that their destruction in a pure ice environment is quite inefficient. Errors in the estimation of σ_{des} are dominated by the uncertainty in the UV flux, and therefore relative values of σ_{des} listed in Table 11 are accurate, but the absolute scale could vary by about a factor of two.

Table 11. Calculated initial UV destruction cross-sections, assuming a lamp flux of ϕ = 1(15) photons cm^{-2} s^{-1}

Molecule	Destruction cross section (cm^2)
CH_4	7.2(-19)
CO_2	5.6(-19)
O_2 [a]	3.2(-18)
CH_3OH	1.6(-18)
H_2CO	6.2(-18)
CO [b]	< 8(-20)

[a] Cross-section for O_2 calculated from the formation rate of O_3; [b] loss of CO is below resolution of measurements.

Table 12. Initial UV formation cross-sections, calculated assuming a lamp flux of ϕ = 1(15) photons cm^{-2} s^{-1}

Experiment	Product	Formation cross section (cm^2)
CO	CO_2	1.3(-20)
CO_2	CO	3.8(-19)
O_2	O_3	2.1(-18)
CH_4	C_2H_6	3.2(-19)
H_2CO	POM [CH_2O] group	3.8(-18)
	CO	2.6(-19)
	HCO	2.1(-20)
CH_3OH	H_2CO	1.1(-18)
	CH_4	4.4(-19)

3.11. Formation cross-sections

Initial cross-sections for the formation of first-order photoproducts, σ_{form} (in cm^2), may be derived from

$$\frac{dN}{dt} = \phi \cdot N_P \cdot \sigma_{form} \quad (2)$$

where N is the abundance of the photoproduct, N_P is the abundance of the parent molecule, and ϕ is the flux of UV photons. Where possible, we have estimated the initial change in N for each species by fitting the first four points (at t = 0, 5, 15, and 60 s) in the plot of abundance vs. time. These values were then used to calculate the initial cross-sections for formation. The results of these calculations are listed in Table 12.

4. Reaction schemes

The main aim of this research is to quantitatively describe the photochemical modifications of astrophysically relevant ices.

For this reason, no in-depth investigation was made of the formation mechanisms of detected photoproducts. In this section, however, we summarize the possible reaction schemes which may explain the presence of observed species in these experiments (some well-established, others more speculative).

4.1. H_2O

Products observed in the H_2O irradiations were OH, HO_2, and H_2O_2. The photochemistry of the water molecule begins with either of these two steps (Okabe 1978):

$$H_2O + h\nu \rightarrow H + OH \quad (1a)$$

$$H_2O + h\nu \rightarrow H_2 + O\,. \quad (1b)$$

Reaction (1b) is of minor importance (see Okabe 1978) and this is supported in our experiments since no H_2 was observed. Subsequent steps then lead to the formation of H_2O_2 and HO_2 as follows:

$$OH + OH \rightarrow H_2O_2 \quad (1c)$$

$$OH + H_2O_2 \rightarrow H_2O + HO_2\,. \quad (1d)$$

Reaction (1c) is the most likely candidate for the production of H_2O_2 in our experiments. The HO_2 molecule, observed here only in long irradiation timesteps, may be produced by reaction (1d) or by photodissociation of H_2O_2 (Okabe 1978 and references therein).

4.2. NH_3

Species produced in the photolysis of NH_3 in these experiments were N_2H_4, NH_2, and H_2. Ammonia has two possible primary photolysis steps:

$$NH_3 + h\nu \rightarrow NH_2 + H \qquad (< 2820\ \text{Å}) \quad (2a)$$

$$NH_3 + h\nu \rightarrow NH + H_2 \qquad (< 2240\ \text{Å})\,, \quad (2b)$$

where reaction (2a) is dominant (Hagen 1982; Okabe 1978). The formation of N_2H_4 may occur as follows:

$$NH + NH_3 \rightarrow N_2H_4 \quad (2c)$$

$$NH_2 + NH_2 \rightarrow N_2H_4\,. \quad (2d)$$

If reaction (2c) is very efficient, then all NH radicals may quickly be lost to the NH_3 matrix to form N_2H_4. Thus we may explain its absence in our IR spectra.

4.3. CH_4

The UV photolysis of solid CH_4 at 10 K in these experiments produced ethane, propane, ethylene (C_2H_4), allene (C_3H_4), larger molecules containing H-C≡C- and H_2C=C- groups, and larger alkanes with 4 to more than 7 C atoms per molecule, which consist of highly branched structures (seen via R-CH_3 and R-CH_2-R stretching and deformation modes). The primary photodissociation pathways for methane involve (Okabe 1978):

$$CH_4 + h\nu \rightarrow CH_3 + H \quad (3a)$$

$$CH_4 + h\nu \rightarrow CH_2 + H_2 \quad (3b)$$

$$CH_4 + h\nu \rightarrow CH + H_2 + H\,. \quad (3c)$$

Subsequent steps involve reactions of CH, CH_2, and CH_3 with each other and with CH_4 (e.g., Okabe 1978; Braun et al. 1970), e.g.:

$$CH + CH_2 \rightarrow C_2H_3 \quad (3d)$$

$$CH_2 + CH_4 \rightarrow C_2H_6 \quad (3e)$$

$$CH_2 + CH_2 \rightarrow C_2H_4 \quad (3f)$$

$$2CH_3 \rightarrow C_2H_6\,. \quad (3g)$$

Large products may evolve from the addition of radicals to unsaturated species or other radicals, such as:

$$CH + C_2H_3 \rightarrow C_3H_4\ (\text{allene}) \quad (3h)$$

$$CH_3 + C_2H_4 \rightarrow C_3H_7 \quad (3i)$$

$$C_3H_7 + CH_3 \rightarrow C_4H_{10}\,. \quad (3j)$$

Such a stepwise building block mechanism seems consistent with the highly branched structures indicated for the large hydrocarbons.

4.4. CO

Products of the CO photolysis experiments were CO_2, C_2O, C_3O, C_3O_2 and C_3. The direct photodissociation of the CO molecule has a threshold wavelength of 1118 Å (Okabe 1978) and falls outside the range of the UV radiation applied (see Sect. 2). The alternative photochemical pathway lies through an electronic excitation of a CO molecule and requires photons with wavelengths shorter than 1470 Å (Hagen 1982 and references therein). The excited CO molecule may react with other CO molecules within the ice matrix to produce CO_2 and C atoms (e.g., Okabe 1978; Luiti et al. 1966) by the reaction

$$CO^* + CO \rightarrow CO_2 + C\,. \quad (4a)$$

Subsequent reactions then occur between the free C atoms and the CO matrix (Okabe 1978). For example:

$$C + CO \rightarrow C_2O \quad (4b)$$

$$C + C_2O \rightarrow C_3O \quad (4c)$$

$$C_2O + CO \rightarrow C_3O_2 \quad (4d)$$

$$3C \rightarrow C_3\,. \quad (4e)$$

4.5. CO_2

The photolysis of CO_2 produces CO, CO_3, C_3O and O_3 in our experiments (Sect. 3.5). At wavelengths less than 2275 Å, CO_2 may photodissociate to form CO and O (Okabe 1978). Secondary reactions of O with CO_2 and with itself lead to CO_3, O_2, and O_3 (e.g., Moll et al. 1966). The CO produced by the direct photolysis of CO_2 may follow the scheme described in Sect. 4.4 (above) to produce the trace of C_3O seen.

4.6. N_2

No products of the N_2 photolysis were clearly identified, although some evidence exists for the formation of the N_3 radical. The wavelength threshold for the photodissociation of N_2 lies at 1270 Å (Okabe 1978), and hence, if this molecule were to photodissociate, then speculatively, the formation of N_3 could take place by addition of an N atom to N_2.

4.7. O_2

The sole photolysis product of O_2 seen in these experiments is O_3, which may be formed after the photodissociation of O_2 (Okabe 1978) and addition of an O atom to O_2.

4.8. H_2CO

New species observed in the UV irradiation of H_2CO are polyoxymethylene (POM) chains, CH_3OH, CH_4, HCO, CO, CO_2, C_3O, H_2, methyl formate (H_3COHCO), and the $HCO[HCOH]_nH_2COH$ polymer. CO and HCO may be formed via the direct photodissociation of H_2CO (Okabe 1978). CO_2, and C_3O would follow from the subsequent photolysis of CO (Reactions 4a - 4c). CH_3OH is most likely formed primarily through

$$H_2CO + h\nu \rightarrow HCOH \quad (8a)$$

$$H_2CO + HCOH \rightarrow CH_3OH + CO \quad (8b)$$

(Kemper et al. 1981). Moreover, H atoms produced by H_2CO photolysis could recombine with H_2CO to form CH_3OH (Hiraoka et al. 1994). The combination of two H_2CO molecules may lead to the formation of methyl formate (CH_3COHCO; Goldanskii et al. 1973). The chains observed, $HCO[CH_2O]_nH_2COH$ (POM) and $HCO[HCOH]_nH_2COH$, are produced through H_2CO polymerization, where the energy produced by UV absorption may overcome the barrier of these reactions.

4.9. CH_3OH

H_2CO, CH_4, methyl formate, HCO, CO, CO_2, and H_2 are formed in the photolysis of solid CH_3OH at 10 K. The first-order products of CH_3OH observed in Sect. 3.9 should be formed directly from its photodissociation:

$$CH_3OH + h\nu \rightarrow H_2CO + H_2 \quad (9a)$$

$$CH_3OH + h\nu \rightarrow CH_4 + O\,. \quad (9b)$$

Reaction (9b) is not observed in the gas phase (von Sonntag 1969), and more research (e.g., the photolysis of CH_3OH in inert matrices) needs to be performed to verify that CH_4 is truly a first-order product of the solid phase photolysis of CH_3OH.

The CH_2OH radical may be formed by hydrogen abstraction (van Sonntag 1969; Jacox 1981):

$$CH_3OH + H \rightarrow CH_2OH + H_2\,. \quad (9c)$$

Subsequent reactions to form HCO, CO, CO_2, and methyl formate follow the scheme of H_2CO (see Sect. 4.8, above). No POM or $HCO[HCOH]_nH_2COH$ formaldehyde polymers are observed in the spectrum of irradiated CH_3OH. Presumably, this is related to the low concentration of H_2CO, which does not exceed 8 % at any stage of the irradiation.

5. Discussion and astrophysical implications

Our experiments show that a large number of new species are produced upon UV photolysis of simple molecules. Among these new molecules are free radicals, and in some cases, large organic species. Our results agree well with earlier experiments involving somewhat more complex ice mixtures, i.e., H_2O:CH_3OH:NH_3:CO (Allamandola et al. 1988), CO:H_2O, CO:NH_3 and CO:CH_4 (Hagen 1982), H_2O:CO:CH_4:NH_3:O_2:N_2 (d'Hendecourt et al. 1986), and H_2O:CO:O_2 (Ehrenfreund et al. 1992). The results presented in Sect. 3 reproduce some of the previously identified species and also present a large number of molecules which had not been observed in earlier experiments. Examples of the latter are H_2O_2 and HO_2 (from H_2O photolysis), N_2H_4 (from NH_3), and CH_3OHCO (from CH_3OH and H_2CO).

This discrepancy between older photolysis experiments with more complex mixtures and those presented here may be due to the absence of species which easily react with the products of photodissociation, increasing the efficiency of other reaction pathways. Also, the less-crowded infrared spectra of our simple ices enable a more sensitive search for new features. The high sensitivity of the spectrometer currently in use in our laboratory, in comparison with instruments employed in the past, could also play a role. Certainly, these many new identifications from initially pure ice samples stress the importance of studying individual ice components before attempting to understand the photochemistry of complex mixtures.

Our results have a number of astrophysical implications. Ramifications reach beyond the solid phase, since volatile species which are photochemically produced in the ice mantles could be injected into the gas phase by desorption mechanisms such as grain mantle explosions and cosmic ray heating (e.g., Shalabiea & Greenberg 1994; Hasegawa & Herbst 1993). In warm dense cores close to star-formation regions, thermal sublimation of the grain mantles becomes significant. A number of species which are identified in our experiments have been found in the gas phase of dense clouds. For example, C_2O and C_3O have both been detected in the dark cloud TMC-1 at abundances of $\sim 10^{-5}$ and $\sim 10^{-6}$ relative to CO, respectively (Ohishi et al. 1991). Methyl formate (CH_3OHCO) has been identified in

the Orion compact ridge and Sgr B2 (regions of ongoing massive star formation) at abundances of 2×10^{-4} and 2×10^{-5} relative to CO, respectively, but has not been found in TMC-1 ($N/N_{CO} < 10^{-5}$, Blake et al. 1987; Irvine et al. 1987). Models of gas-phase chemistry which include surface reactions and desorption from grains fall short by many orders of magnitude in reproducing the observed C_2O abundance, although the C_3O abundance may be reasonably reproduced (e.g., Hasegawa & Herbst 1993). It seems quite possible that photoproduction of these volatile species in the apolar, CO-rich phase of interstellar ices followed by desorption could be an important source for the observed gas-phase abundances. Methyl formate, on the other hand, may be efficiently produced in the gas phase in star-forming regions (Caselli et al. 1993; Charnley et al. 1992), and the significance of direct injection from the grains is unclear in this case.

The high destruction rate observed for H_2CO (see Table 11) supports the conclusions by Schutte et al. (1996) that the generally low observed abundance of H_2CO in interstellar ices could be related to its high susceptibility to photochemical destruction. With the destruction cross-section indicated in Table 11, 90 % of our H_2CO ice sample is destroyed at a dose of $R \approx 0.8$. Such doses could be quite realistic for grains near protostellar objects (Tegler et al. 1995; Schutte et al. 1996).

The very efficient polymerization of formaldehyde upon ultraviolet photolysis has been observed previously (Goldanskii et al. 1973; Mansueto & Wight 1989; Mansueto et al. 1989). It must be noted that formaldehyde is an efficient source of organic species even at the relatively small concentrations produced by irradiation of solid methanol: $\sim$ 26 % of the initial CH_3OH has converted into methyl formate with H_2CO as intermediate after 1 hr of irradiation. Our results show clearly that under UV photolysis, formaldehyde would be an efficient producer of organic molecules in icy grain mantles. Similar results have also been found in more complex ice mixtures (Bernstein et al., private communication). This type of reaction mechanism may also play a role in the formation of organic materials which have been observed in comets and the diffuse interstellar medium.

The continuous increase in complexity with irradiation dose for the CH_4 sample could have some interesting implications for the evolution of organic species in the interstellar medium. Although this experiment may indicate that methane photolysis is an efficient source of organic species in interstellar ices, it remains to be investigated whether such a high yield is obtained from a mixture of CH_4 with other ice components, such as CO or H_2O. Additionally, it is intriguing to consider our experiment as a template for the evolution of the refractory organic grain mantles observed in the diffuse interstellar medium (e.g., Sandford et al. 1991; Pendleton et al. 1990; Tielens & Allamandola 1987). It appears that under the influence of the strong ambient UV flux in the diffuse environment, a hydrocarbon material may increase in complexity. Such an evolution could be related to the durability of this organic material, which appears to survive for timescales $\sim 10^7 - 10^8$ yr in the harsh environment of the diffuse medium (Greenberg 1982).

Acknowledgements. We would like to thank M. de Groot for his continued service and valued contributions to the Leiden Obseratory Laboratory. We are grateful to E.F. van Dishoeck and J.M. Greenberg for their many comments and helpful discussions, as well as to F. Salama for his advice on working with Ar in UV experiments. This work benefitted from NASA grants NAGW 4039 and NGR 33-018-148, and a PIONIER grant from the Netherlands Organization for Scientific Research (NWO). W.A. Schutte also acknowledges support from ASTRON and SRON. P. Ehrenfreund is a recipient of the European Community fellowship ERBCHBICT940939.

References

Acquista N., Schoen L.J., Lide D.R., 1968, J. Chem. Phys 48, 1534
Agarwal V.K., Schutte W.A., Greenberg J.M., et al., 1985, Origins of Life 16, 21
Allamandola L.J., Sandford S.A., Valero G.J., 1988, Icarus 76, 225
Allamandola L.J., Sandford S.A., Tielens A.G.G.M., Herbst T.M., 1992, ApJ 399, 134
Ausloos P., Rebbert, R.E., Lias, S.G., 1965, J. Chem. Phys. 42, 540
Blake G.A., Sutton E.C., Masson C.R., Phillips T.G., 1987, ApJ 315, 621
Boogert A., et al., 1996, in prep
Braun W., Baas A.M., Pilling M., 1970, J. Chem. Phys. 52, 5131
Brecher C., Halford R.S., 1961, J. Chem. Phys. 35, 1109
Brewer L., Wang J.L., 1972, J. Chem. Phys. 56, 759
Briggs R., Ertem G., Ferris J.P., et al., 1992, Origins of Life and Evolution of the Biosphere 22, 287
Brown P.D., Charnley S.B., 1990, MNRAS 244, 432
Cairns B.R., Pimentel G.C., 1965, J. Chem. Phys. 43, 3432
Caselli P., Hasegawa T.I., Herbst E., 1993, ApJ 408, 548
Charnley S.B., Tielens A.G.G.M., Millar T.J., 1992, ApJ 399, L71
Chesters M.A., McCash E.M., 1987, Spectrochim. Acta 43A, 1625
Comeford J.J., Gould J.H., 1960, J. Mol. Spectr. 5, 474
DeKock R.L., Weltner W., 1971, J. Am. Chem. Soc. 93, 7106
d'Hendecourt L.B., Allamandola L.J., 1986, A&AS 64, 453
d'Hendecourt L.B., Jourdain de Muizon M., 1989, A&A 223, L5
d'Hendecourt L.B., Allamandola L.J., Greeneberg J.M., 1986, A&A 152,130
Duncan J.L., McKean D.C., Mallinson P.D., 1973, J. Mol. Spectr. 45, 221
Ehrenfreund P., Breukers R., d'Hendecourt L., Greenberg J.M., 1992, A&A 260, 431
Ehrenfreund P., Gerakines P.A., Schutte W.A., van Hemert M.C., van Dishoeck E.F., 1996, A&A, submitted
Fan L., Ziegler T., 1992, J. Chem. Phys. 96, 9005
Gerakines P.A., Schutte W.A., Greenberg J.M., van Dishoeck, 1995, A&A 296, 810
Giguère P.A., Harvey K.B., 1959, J. Mol. Spectr. 3, 36
Goldanskii V.I., Frank-Kamenetskii M.D., Barkalov I.M., 1973, Science 182, 1344
Gredel R., Lepp S., Dalgarno A., Herbst E., 1989, ApJ 347, 289
Greenberg J.M., 1973, in: Molecules in the Galactic Environment, M.A. Gordon & L.E. Snyder (eds.), Wiley, New York, p. 94
Greenberg J.M., 1982, in: Submillimetre Wave Astronomy, J.E. Beckman & J.P. Phillips (eds.), Cambridge University Press, p. 262
Greenberg J.M., Yencha A.J., 1973, in: Interstellar Dust and Related Topics, Proceedings of IAU symp. No. 52, J.M. Greenberg & H.C. van de Hulst (eds.)
Grim R.J.A., d'Hendecourt L.B., 1986, A&A 167, 161
Grim R.J.A., Greenberg J.M., 1987, ApJ 321, L91

Grim R.J.A., Greenberg J.M., de Groot M.S., et al., 1989, A&AS 78, 161
Hagen W., 1982, PhD. thesis, University of Leiden
Hagen W., Allamandola L.J., Greenberg J.M. 1979, Ap&SS 65, 215
Hasegawa T.I., Herbst E., 1993, MNRAS 261, 83
Hasegawa T.I., Herbst E., Leung C.M., 1992, ApJS 82, 167
Hiraoka K., Ohashi N., Kihare Y., et al., 1994, Chem. Phys. Lett. 229, 408
Hudgins D.M., Sandford S.A., Allamandola L.J., Tielens A.G.G.M., 1993, ApJS 86, 713
Irvine W.M., Goldsmith P.F., Hjalmarson A., 1987, in: Interstellar Processes, D.J. Hollenbach & H.A. Thronson (eds.), Reidel, Dordrecht, 561
Jacox M.E., 1981, Chem. Phys. 59, 213
Jacox M.E., Milligan D.E., 1972, J. Mol. Spectr. 42, 495
Jacox M.E., Milligan D.E., Moll N.G., Thompson W.E., 1965, J. Chem. Phys. 43, 3734
Jenniskens P., Baratta G.A., Kouchi A., et al., 1993, A&A 273, 583
Kemper M.J.H., Hoeks C.H., Buck H.M., 1981, J. Chem. Phys. 74, 5749
Kissel J., Krueger F.R., 1987, Nature 326, 755
Klein M.L., Venables J.A., eds., 1976, Rare Gas Solids, Vol. 1, Academic Press, London
Lacy J.H., Baas F., Allamandola L.J., et al., 1984, ApJ 276, 543
Luiti G., Dondes S., Harteck P., 1966, J. Chem. Phys. 44, 4051
Maki A.G., Toth R.A., 1965, J. Mol. Spectr. 17, 136
Mansueto E.S., Wight C.A., 1989, J. Am. Chem. Soc. 111, 1900
Mansueto E.S., Ju C.-Y., Wight C.A., 1989, J. Phys. Chem. 93, 2143
Mathis J.S., Mezger P.G., Panagia N., 1983, A&A 128, 212
Millar T.J., Herbst E., Charnley S.B., 1991, ApJ 369, 147
Milligan D.E., M.E. Jacox, 1965, J. Chem. Phys. 43, 4487
Milligan D.E., M.E. Jacox, 1971, J. Chem. Phys. 54, 927
Milligan D.E., Brown H.W., Pimentel G.C., 1956, J. Chem. Phys. 25, 1080
Moll N.B., Ckitter D.R., Thompson W.E., 1966, J. Chem. Phys. 45, 4469
Ohishi M., Suzuki H., Isikawa S.-I., et al., 1991, ApJ 380, L39
Okabe H., 1978, Photochemistry of Small Molecules, Wiley, New York
Pacansky J., Bargon J., 1975, J. Am. Chem. Soc. 97, 6896
Pacansky J., Koch W., Miller M.D., 1981, J. Am. Chem. Soc. 113, 317
Pendleton Y.J., Sandford S.A., Allamandola L.J., Tielens A.G.G.M., Sellgren K., 1994, ApJ 437, 683
Pouchert C.J. (ed.), 1981, The Aldrich Library of Infrared Spectra, edition III, Aldrich Chemical Company, Millwaukee
Prasad S.S., Tarafdar S.P., 1983, ApJ 267, 603
Rosengren K., Pimentel G.C., 1965, J. Chem. Phys. 43, 507
Roux J.A., Wood B.E., 1983, J. Opt. Soc. Am. 73, 1181
Sandford S.A., Allamandola L.J., 1990, ApJ 355, 357
Sandford S.A., Allamandola L.J., 1993, ApJ 409, L65
Sandford S.A., Allamandola L.J., Tielens A.G.G.M., Valero L.J., 1988, ApJ 329, 498
Sandford S.A., Allamandola L.J., Tielens A.G.G.M., et al., 1991, ApJ 371, 607
Saussey J., Lamotte J., Lavalley J.C., 1976, Spectrochim. Acta 32A, 763
Schutte W.A., 1988, PhD. Thesis, University of Leiden
Schutte W.A., Greenberg J.M., 1991, A&A 244, 190
Schutte W.A., Allamandola L.J., Sandford S.A., 1993, Icarus 104, 118
Schutte W.A., Gerakines P.A., Geballe T.R., van Dishoeck E.F., Greenberg J.M., 1996, A&A, submitted
Seloudoux R., Soussen-Jacob J., Vincent-Geisse J., 1979, Chem. Phys. 40, 257
Shalabiea O.M., Greenberg J.M., 1994, A&A 290, 266
Skinner C.J., Tielens A.G.G.M., Barlow M.J., Justtanont K., 1992, ApJ 399, L79
Smith M.A.H., Rinsland C.P., Fridovich B., Rao K.N., 1985, in: Molecular Spectroscopy- Modern research, Vol. III, K.N. Rao (ed.), Academic Press, London, p. 111
Smith R.G., Sellgren K., Tokunaga A.T., 1989, ApJ 344, 413
Smith W.H., Leroi G.E., 1966, J. Chem. Phys. 45, 1767
Sodeau J.R., Lee E.K., 1978, Chem. Phys. Lett. 57, 71
Strazulla G., Baratta G.A., 1992, A&A 266, 434
Sternberg A., Dalgarno A., Lepp S., 1987, ApJ 320, 676
Tegler S.C., Weintraub D.A., Rettig T.W., et al., 1995, ApJ 439, 279
Tielens A.G.G.M., Allamandola L.J., 1987, in: Interstellar Processes, D.J. Hollenbach & H.A. Thronson (eds.), Reidel, Dordrecht, p. 397
Tielens A.G.G.M., Tokunaga A.T., Geballe T.R., Baas F., 1991, ApJ 381, 181
von Sonntag C., 1969, Forschr. Chem. Forsch. 13, 333
Walker J.F., 1964, Formaldehyde, Reidhold, New York
Weber P., Greenberg J.M., 1985, Nature 316, 403
Wexler A.S., 1967, Appl. Spectr. Rev. 1, 29
Whittet D.C.B., Adamson A.J., Duley W.W., Geballe T.R., McFadzean A.D., 1989, MNRAS 241, 707
Willner S.P., Gillett F.C., Herter T.L., et al., 1982, ApJ 253, 174
Wormhoudt J., McCurdy K.E., 1989, Chem. Phys. Lett. 156, 47
Youngquist M.J., Crawford B., Overend J., 1979, J. Phys. Chem. 83, 2638

This article was processed by the author using Springer-Verlag LaTeX A&A style file *L-AA* version 3.